Orthogonal machining introduced microstructure modification in AA7150-T651 aluminium alloy

DOI:
10.1016/j.matchar.2016.11.015

Document Version
Accepted author manuscript

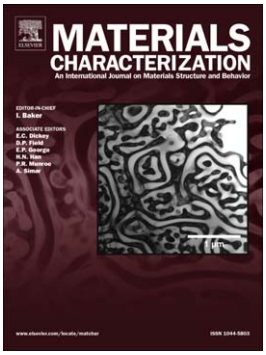

Orthogonal machining introduced microstructure modification in AA7150-T651 aluminium alloy

Bing Liu, Xiaorong Zhou, Xinxin Zhang

PII: S1044-5803(16)30925-1
DOI: doi:10.1016/j.matchar.2016.11.015
Reference: MTL 8455

To appear in: *Materials Characterization*

Received date: 6 September 2016
Revised date: 12 November 2016
Accepted date: 14 November 2016

Please cite this article as: Liu Bing, Zhou Xiaorong, Zhang Xinxin, Orthogonal machining introduced microstructure modification in AA7150-T651 aluminium alloy, *Materials Characterization* (2016), doi:10.1016/j.matchar.2016.11.015

Orthogonal machining introduced microstructure modification in AA7150-T651 aluminium alloy

Bing Liu, Xiaorong Zhou*, Xinxin Zhang

Corrosion and Protection Centre, School of Materials, the University of Manchester, Sackville Street, Manchester, M13 9PL, UK

*xiaorong.zhou@manchester.ac.uk

Abstract: In the present work, orthogonal machining is simulated on AA7150-T651 aluminium alloy by cutting using ultramicrotomy. The simulation has successfully reproduced the interaction between the tool and the workpiece during industrial machining process and the associated shear deformation introduced to the workpiece. Within the tertiary shear zone, near-surface deformed layers, characterized by ultrafine grains with diameters less than 100 nm, are generated on the workpiece. The thickness of the deformed layer ranges from approximately 200 nm to 400 nm, depending on the machining parameters. Increased cutting thickness or cutting speed results in the formation of a near-surface deformed layer with increased thickness. Machining with 0 degree clearance angle results in thicker deformed layer compared with that at 45 degrees clearance angle.

Key words: Aluminium alloy; orthogonal machining; cutting; near-surface deformed layer.

Bing Liu
Email: bing.liu@manchester.ac.uk

Corresponding author: Xiaorong Zhou
Email: xiaorong.zhou@manchester.ac.uk
Telephone: 00441613064832

Xinxin Zhang
Email: xinxin.zhang@manchester.ac.uk

Orthogonal machining introduced microstructure modification in AA7150-T651 aluminium alloy

Bing Liu, Xiaorong Zhou*, Xinxin Zhang

Corrosion and Protection Centre, School of Materials, the University of Manchester, Sackville Street, Manchester, M13 9PL, UK

*xiaorong.zhou@manchester.ac.uk

Abstract: In the present work, orthogonal machining is simulated on AA7150-T651 aluminium alloy by cutting using ultramicrotomy. The simulation has successfully reproduced the interaction between the tool and the workpiece during industrial machining process and the associated shear deformation introduced to the workpiece. Within the tertiary shear zone, near-surface deformed layers, characterized by ultrafine grains with diameters less than 100 nm, are generated on the workpiece. The thickness of the deformed layer ranges from approximately 200 nm to 400 nm, depending on the machining parameters. Increased cutting thickness or cutting speed results in the formation of a near-surface deformed layer with increased thickness. Machining with 0 degree clearance angle results in thicker deformed layer compared with that at 45 degrees clearance angle.

Highlights:

1. Orthogonal machining modifies the microstructure within the near-surface region of workpiece.
2. The near-surface deformed layers, characterized by ultrafine grains, are approximately 200-400 nm thick.
3. Machining parameters have significant effect on the formation of the near-surface deformed layer.

Keywords: Aluminium alloy; orthogonal machining; cutting; near-surface deformed layer.

1. Introduction

Extensive research on the microstructure evolution within the near-surface region where high shear deformation occurs during alloy fabrication or structure manufacturing processes, including rolling, mechanical grinding and polishing, has been reported recently [1-9]. Generally, near-surface deformed layers, exhibiting distinct microstructural features in

comparison with the underlying bulk material, including the ultrafine equiaxed grains, redistribution of alloying elements and elements segregation at the grain boundaries, are formed on various metallic materials during the fabrication processes. The corrosion resistance, forming performance, as well as optical properties, could be significantly affected by the presence of the near-surface deformed layers [1, 4, 9-12].

Various factors are associated with the formation of the near-surface deformed layer, of which the high level of shear stresses and temperature are most dominant [2-6]. Humphreys and Hatherly [13] proposed, based on the observation on materials undergoing high shear deformation processes, the dislocation network generated during severe deformation leads to the formation of sub-grain structures within the grain. Such structures with low-angle boundaries will finally become separate ultrafine grains as deformation progresses. The grain refinement process is referred to as continuous dynamic recrystallization.

It is known that shear stress of significant magnitude is introduced to the workpiece during machining operation [14-16]. Consequently, shear zones develop within the workpiece subjected to machining operation, including the primary shear zone, the secondary shear zone and the tertiary shear zone [17]. Within the tertiary shear zone, i.e. the region immediately beneath the machining tool, shear deformation occurs as a consequence of the frictional interaction between the tool and the workpiece. However, little on the influence of the frictional interaction on the microstructure within the region immediately beneath the machining tool has been reported. The present research investigates the microstructure evolution within the near-surface region of the workpiece during machining in order to correlate the microstructure modification within the region immediately beneath the machining tool with the machining parameters.

2. Materials and methods

AA7150-T651 aluminium alloy with the chemical composition listed in Table 1 is used in the present study. As the near-surface deformed layer may have already been introduced on the as-received alloy by the previous fabrication process, the alloy was alkaline etched before machining. The sample was immersed in a 10 wt. % NaOH solution at 60 °C for 60 seconds and then was immersed in 30 vol. % HNO_3 solution for 20 seconds for desmutting.

In order to precisely control the machining parameters, including cutting thickness, cutting speed and clearance angle, orthogonal machining, referred to as machining thereafter, was simulated using a Leica EM UC6 ultramicrotome with a glass knife as the cutting tool. Microstructure characterization of the region immediately beneath the cutting knife on the workpiece was carried out by scanning electron microscopy (SEM) and transmission electron microscopy (TEM).

Table 1 Chemical composition of the AA7150 aluminium alloy [wt. %]

Zn	Cu	Mg	Zr	Fe	Si	Ti	Al
6.90	2.17	2.61	0.12	0.06	0.06	0.04	Bal.

3. Results

3.1 Microstructure modification in the near-surface region during orthogonal machining

For the characterization of the alloy microstructure within the near-surface region immediately beneath the cutting knife, the machining parameters are as follows: cutting thickness is 1 μm; cutting speed is 1.00 mm s^{-1}; clearance angle is 0 degree.

Fig. 1(a) shows the SEM micrograph of the alloy surface on which the machining operation was terminated half-way across the surface, revealing a relatively smooth surface of the alloy after cutting, as well as the continuous and curled chip attached to the machined surface at the location where the cutting operation was terminated. Fig. 1(b) displays the area indicated by the dashed line frame in Fig. 1(a) at an increased magnification, showing the surface finish achieved by cutting while the chip is out of focus in the micrograph. Track-like surface feature is revealed in the micrograph. The distance between two neighbouring tracks is in nano-scale but not uniform. These tracks indicate the subtle surface variation, related to the edge profile of the cutting knife. Fig. 1(c) shows the scanning electron micrograph of the cross section of the region near the chip. A curled chip is evident. Fig. 1(d) exhibits the area indicated by the dashed line frame in Fig. 1(c) at an increased magnification. On the cross section of the chip, short inclined lines are evident, as indicated by the dashed line arrow in Fig. 1(d), indicating the presence of the shear bands introduced by high degree of shear deformation of the alloy within the primary shear zone [18]. Alloy within the chip was shearing significantly along the direction indicated by the shear bands, and as a result, the curled chip was formed and departed from the machined surface.

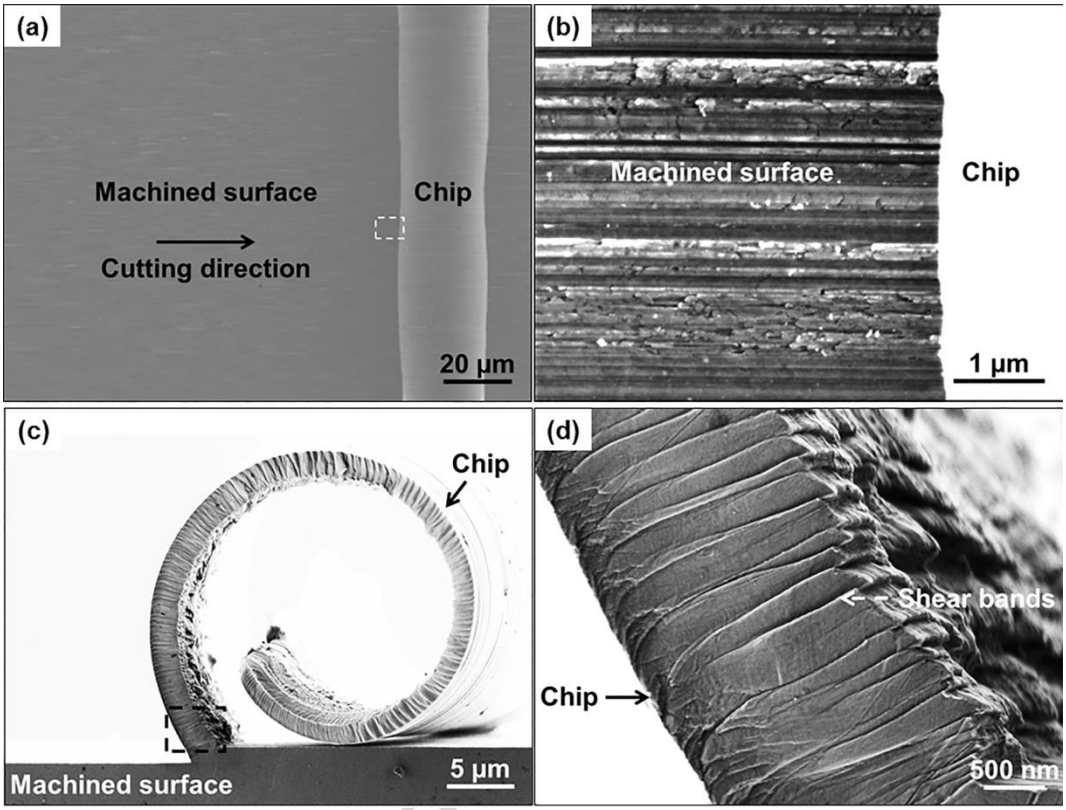

Fig. 1 Scanning electron micrographs of the AA7150-T651 aluminium alloy surface after machining: (a) the machined surface and chip formation; (b) the area indicated by the dashed line frame in (a) at an increased magnification; (c) the cross section; and (d) the area indicated by the dashed line frame in (c) at an increased magnification, showing shear bands within the chip.

However, the deformation of the alloy within the tertiary shear zone [18], which affects the microstructure within the near-surface region on the workpiece, is not obvious in the SEM micrograph of Fig. 1(c). Further investigation was carried out using transmission electron microscopy. Fig. 2(a) exhibits the ultramicrotomed cross section of the etched AA7150-T651 aluminium alloy before orthogonal machining. Fine precipitates are evident within the large grain, which are the $MgZn_2$ precipitates formed in the alloy in T651 temper, as indicated by arrows in the micrograph. Fig. 2(b) shows the TEM micrograph of the cross section of the region immediately beneath the machined surface, and Fig. 2(c) exhibits the region indicated by the dashed line frame in Fig. 2(b) at an increased magnification. Ultrafine grains with the dimensions less than 100 nm, distinguished by the diffraction contrast, are evident in Figs. 2 (b) and (c). The $MgZn_2$ precipitates, which are evident in the region immediately beneath the surface of the etched AA7150-T651 aluminium alloy, are absent within the near-surface region of the machined AA7150-T651 aluminium alloy. Such phenomenon can be explained by the relatively higher temperature generated during machining within the near-surface region of the workpiece, which led to the dissolution of the fine precipitates within the region immediately beneath the cutting knife during machining.

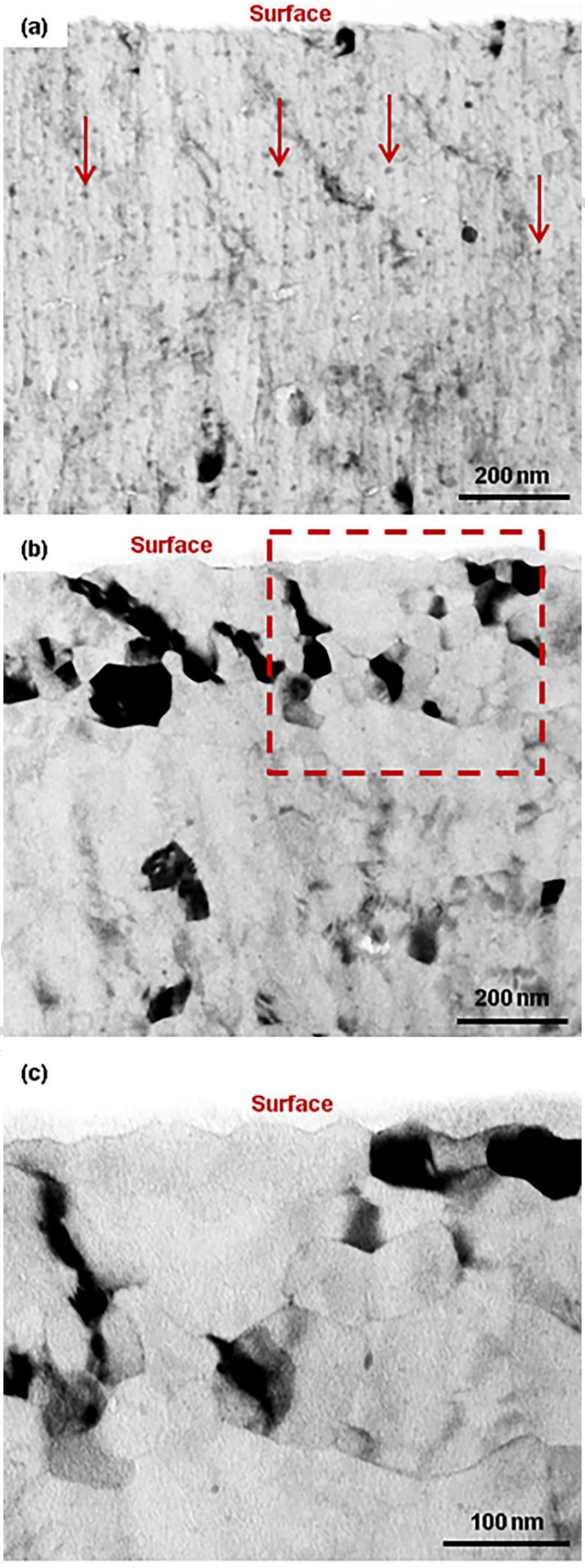

Fig. 2 Transmission electron micrographs of the cross sections of the AA7150-T651 aluminium alloy: (a) before orthogonal machining, with the fine precipitates being indicated by arrows; (b) after orthogonal machining; and (c) the region indicated by the dashed line frame in (b) at an increased magnification.

3.2 The influence of the machining parameters

Machining with various operation parameters was also performed and the corresponding microstructure modification introduced within the region immediately beneath the cutting tool was characterized.

3.2.1 Cutting thickness

Machining was carried out on the AA7150-T651 aluminium alloy with different cutting thicknesses, while other parameters were kept the same, i.e. cutting speed was 1.00 mm s^{-1} and clearance angle was 0 degree. Fig. 3(a) displays the TEM micrograph of the near-surface region and the bulk alloy after machining with the cutting thickness of 0.5 μm. A continuous near-surface deformed layer with the thickness of approximately 200 nm is evident, where ultrafine grains with the dimensions up to 100 nm are distinguished by the diffraction contrast. Large grains are evident in the underlying bulk alloy. Fig. 3(b) shows the TEM micrograph of the cross section of the alloy after machining with the cutting thickness of 1 μm. A thicker near-surface deformed layer of approximately 300 nm is revealed. Within the deformed layer, grains with diameters of less than 100 nm are evident.

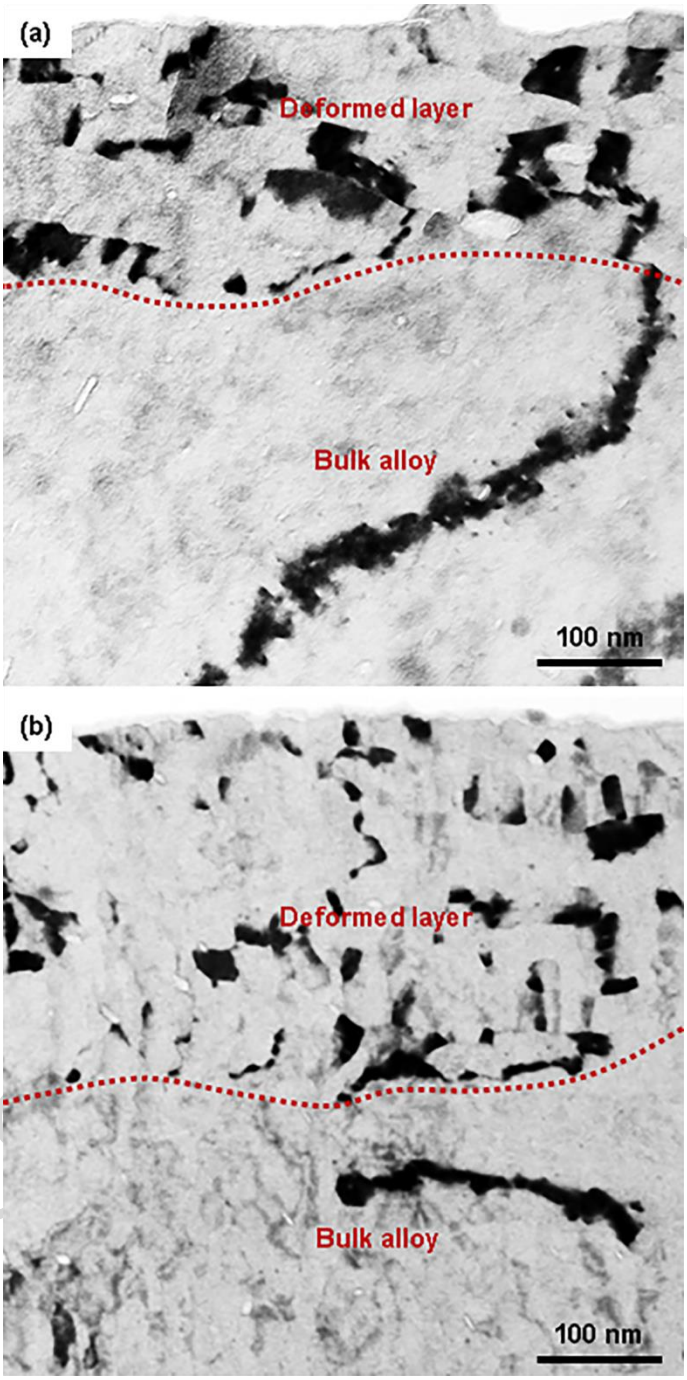

Fig. 3 Transmission electron micrographs of the cross sections of the AA7150-T651 aluminium alloy after machining with a cutting speed of 1.00 mm s^{-1} and a clearance angle of 0 degree: (a) 0.5 µm cutting thickness; and (b) 1 µm cutting thickness.

3.2.2 Cutting speed

Orthogonal machining was also performed with different cutting speeds, when other operation parameters were kept the same, i.e. cutting thickness was 1 μm and clearance angle was 0 degree. Fig. 4(a) shows the TEM micrograph of the cross section of the near-surface region of the workpiece after machining with the cutting speed of 1.00 mm s^{-1}, revealing grains less than 100 nm in diameter. The near-surface deformed layer formed under this condition is approximately 300 nm in thickness. Fine precipitates, less than 10 nm in diameter, are evident in the bulk alloy as dark spots indicated by arrows in the micrograph. Fig. 4(b) displays the TEM micrograph of the cross section of the workpiece after machining with the cutting speed of 2.00 mm s^{-1}. Again, an approximately 400 nm thick near-surface deformed layer characterized by ultrafine grains with diameter up to 100 nm is present beneath the machined surface. Fine precipitates are evident in the bulk alloy. Interestingly, the fine precipitates indicated by arrows are also evident in the deep region of the near-surface deformed layer, indicating that there is a temperature gradient with the workpiece surface experiencing the maximum temperature [19] and the temperature in the deeper region of the near-surface region is not sufficiently high to dissolve the hardening $MgZn_2$ precipitate. Fig. 4(c) shows the TEM micrograph of the cross section of the workpiece after machining with the cutting speed of 3.00 mm s^{-1}. The thickness of the near-surface deformed layer is increased to more than 400 nm.

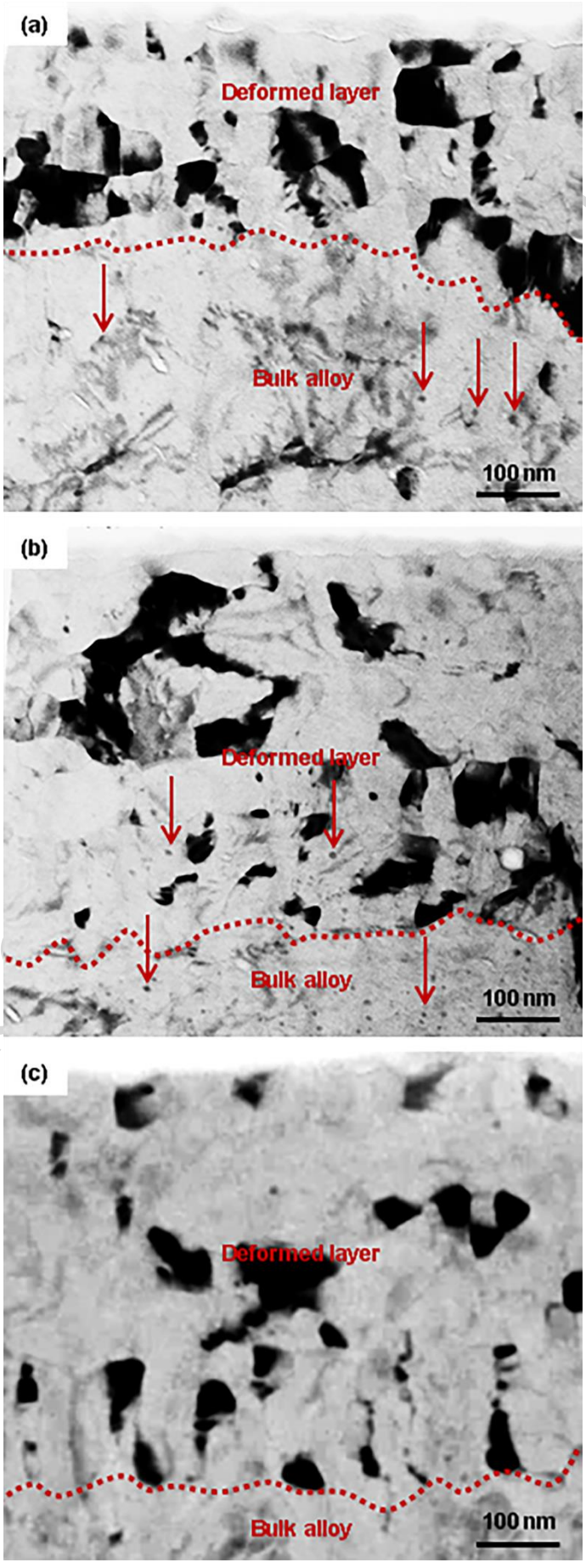

Fig. 4 Transmission electron micrographs of the cross sections of the workpiece after machining with cutting thickness of 1 μm and clearance angle of 0 degree: (a) cutting speed is 1.00 mm s^{-1}; (b) cutting speed is 2.00 mm s^{-1}; and (c) cutting speed is 3.00 mm s^{-1}.

3.2.3 Clearance angle

The influence of clearance angle on the microstructure modification within the near-surface region on the workpiece during orthogonal machining was assessed by cutting with different clearance angles, i.e. 0 degree and 45 degrees, when other operation parameters were kept the same: the cutting thickness and the cutting speed were 1 μm and 1.00 mm s^{-1}, respectively.

Fig. 5(a) displays the TEM micrograph taken from the cross section of the alloy machined with the clearance angle of 0 degree. An approximate 350-400 nm thick deformed layer was introduced by the machining process under the selected condition. Again, the deformed layer is featured by the presence of ultrafine grains less than 100 nm in diameter. Fig. 5(b) shows the deformed layer on the alloy subjected to machining with the clearance angle of 45 degrees, revealing a relatively small thickness of approximately 300 nm. This suggests that the higher clearance angle introduces relatively low level frictional interaction between the cutting knife and the workpiece, resulting in relatively thin near-surface deformed layer. Fine precipitates can be observed in the bulk alloy, as indicated by arrows in both micrographs. Again, such precipitates are absent within the near-surface deformed layers in both micrographs.

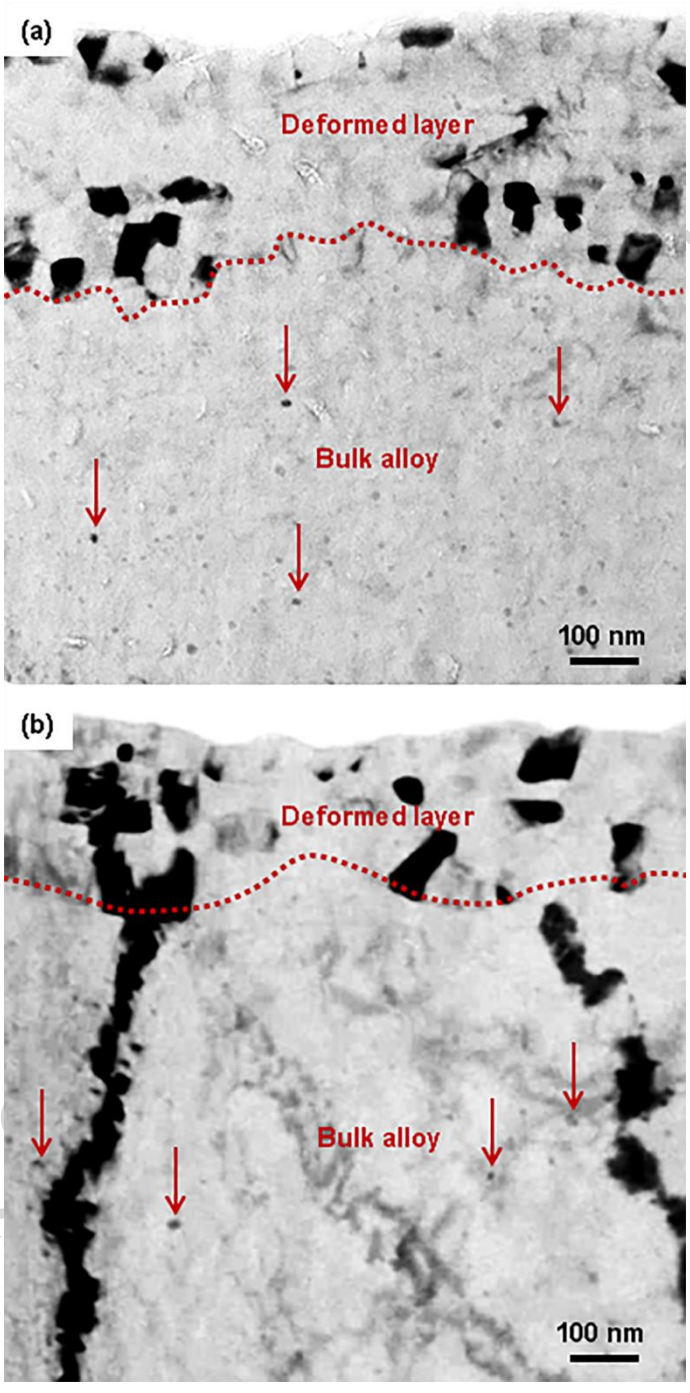

Fig. 5 Transmission electron micrographs of the cross sections of the alloy subjected to machining with the cutting thickness of 1 μm and cutting speed of 1.00 mm s^{-1}: (a) clearance angle is 0 degree; and (b) clearance angle is 45 degrees.

4. Discussion

Fig. 6 displays the transmission electron micrograph of the cross section of the near-surface deformed layer introduced by an industrial-scale machining operation on the AA7150-T651 aluminium alloy. The alloy was subjected to milling with the rotation speed of 4000 rpm and the feed rate of 1000 mm min^{-1}. The cutting thickness is 1 mm. The diameter of the cutter is 160 mm. The ultrafine, equiaxed grains within the approximately 500 nm thick deformed layer are clearly revealed in Fig. 6. It is evident that the characteristics of the near-surface deformed layer introduced by the industrial-scale machining process and the cutting process employed in the present work are the same, suggesting that the cutting process employed in the present work successfully simulated the interaction between the tool and the material beneath the tool during the industrial machining process and the associated deformation introduced to the workpiece.

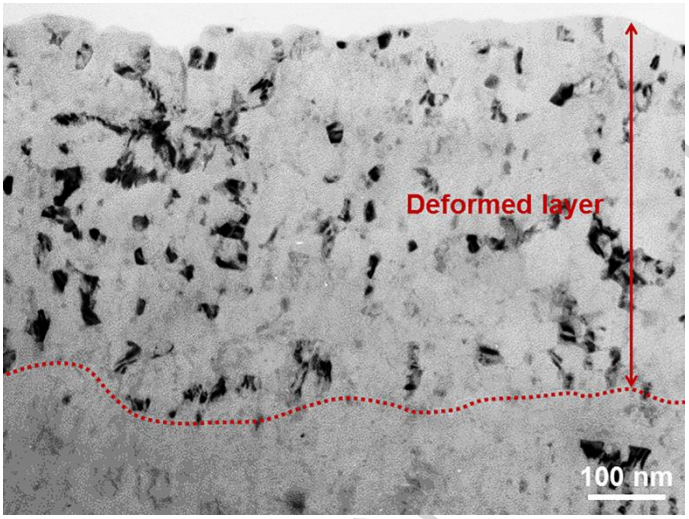

Fig. 6 Transmission electron micrograph of the cross section of the near-surface deformed layer on AA7150-T651 aluminium alloy, introduced by the industrial-scale machining process.

4.1 Chip formation

The development of the primary shear zone on the workpiece undergoing machining is illustrated in Fig. 7. The maximum shear stresses occur at 45 degrees to the direction of the compressive force **F** exerted on the workpiece, i.e. along AB or CD directions as indicated in Fig. 7(a). Consequently, shear planes develop at AB and CD, and the material is sheared along these two directions. However, when the compressive force **F** is acting only on part of the workpiece, as shown in Fig. 7(b), maximum shear stresses and shear planes are generated along AB and CD; but shear deformation of the workpiece only takes place along CD, since the shear deformation along AB is inhibited by the large volume of material in the bulk region. The machining process, as shown in Fig. 7(c), is similar to the process displayed in Fig. 7(b). Once the direction of the cutting force **F** is determined, maximum shear stresses are generated at 45 degrees to the direction of the cutting force. Thus, the position of the primary shear zone can be determined as well, which is inclined at 45 degrees to the cutting force, as indicated by CD in Fig. 7(c), resulting in the shear bands in the chips.

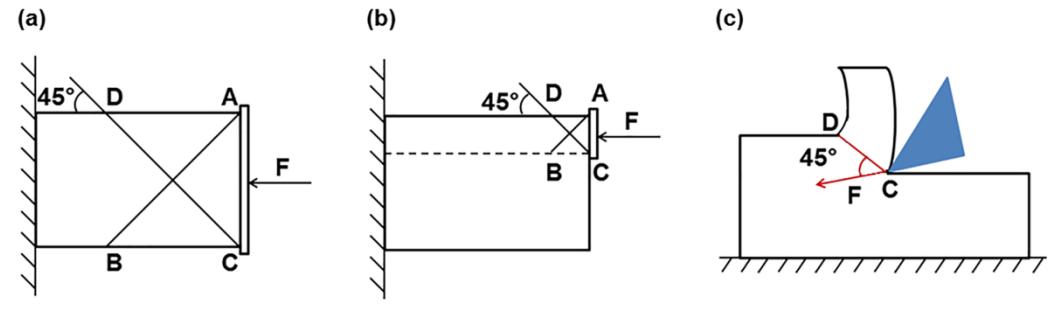

Fig. 7 Schematic diagrams showing the relationship between the maximum shear stresses and the force acting on the workpiece: (a) compressive force acting on a work pirece; (b) compressive force acting on part of a work pirece; and (c) cutting process. **F** represnets the compressive force (in (a) and (b)) and the cutting force (in (c)), and the lines AB and CD indicate the directions of maximum shear stresses.

Further to the above discussion, analysis was also undertaken based on the Mechant's bubble model of chip formation and Black-Huang stack-of-cards model of shear deformation in orthogonal metal cutting [20], as shown in Figs. 8 (a) and (b). Material within the chip undergoes severe shear deformation, leading to the elongation of grains along a certain direction, called shear front direction φ. Fig. 8(c) illustrates the schematic diagram based on the SEM micrograph of the cross section of AA7150-T651 aluminium alloy, indicating the shear deformation of the AA7150-T651 aluminium alloy during cutting. From the micrograph, shear bands are evident, indicated by the two arrays of lines labelled as A and B. The type A bands are present almost through the entire cross section of the chip. These bands are generated by the shear deformation of the alloy within the primary shear zone. The inclination direction of the type A bands indicates the shear front direction, defined as φ. Alloy within the primary shear zone was shearing significantly. As cutting proceeded, increasing volume of alloy was cut and heavily sheared along the shear front direction and consequently the chip was formed in curled shape which finally departed from the surface of the workpiece. The type B bands are only evident along the edge of the chip, inclined along a different direction to those of type A, revealing the presence of the shear bands within the region near the tool/chip interface. Such shear bands are caused by the extensive shear deformation within the secondary shear zone [18] as a consequence of the frictional contact between the chip and the rake face of the cutting tool, as indicated in Fig. 8(c).

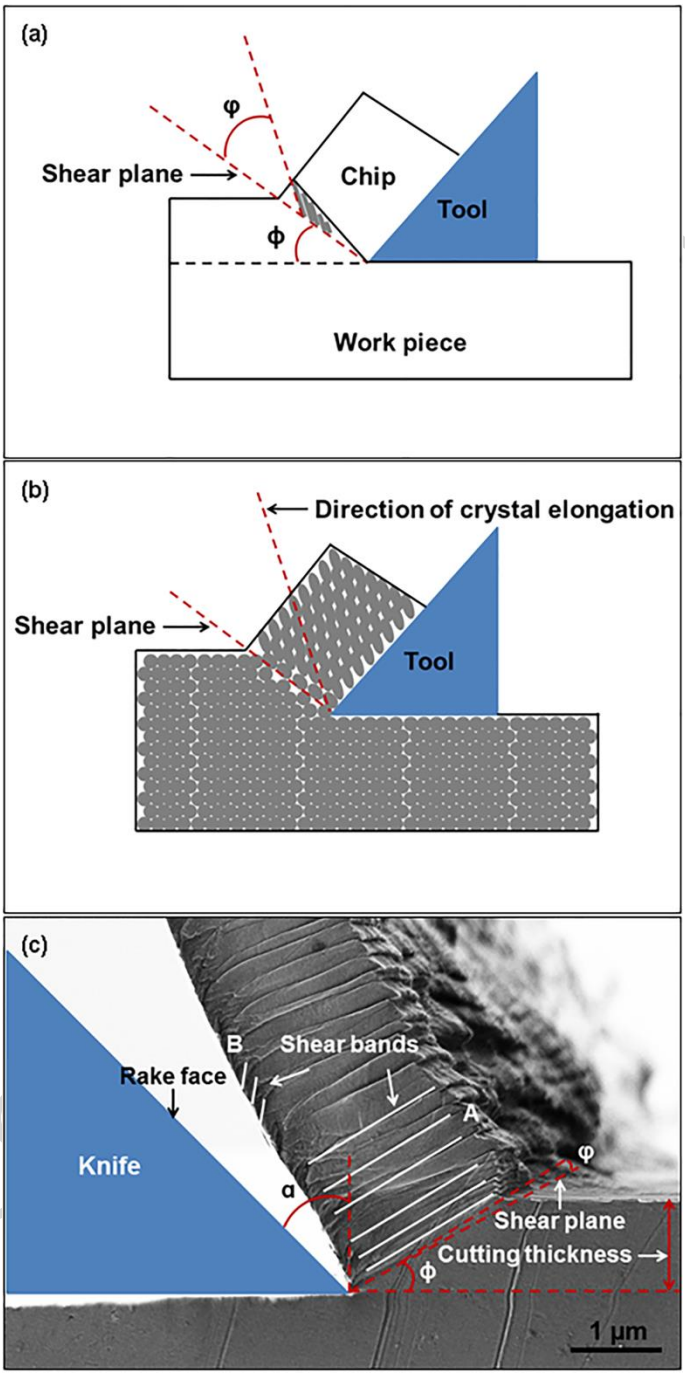

Fig. 8 (a) Mechant's bubble model of chip formation [20]; (b) Black-Huang stack-of-cards model of shear deformation in orthogonal metal cutting [20]; and (c) schematic diagram of orthogonal machining, illustrating the deformation of AA7150-T651 aluminium alloy and the chip formation. ϕ and φ represnet the onset of shear plane angle, and the shear front direction, respectively, and a indicates the rake angle.

4.2 Grain refinement

As revealed in the previous sections, ultrafine grains (≤ 100 nm) are introduced by the machining process to the near-surface region of the workpieces, and the fine strengthening precipitates ($MgZn_2$) that are present in the T651 temper are largely dissolved within the near-surface deformed layers during the machining process. As described, when the tool is moving on the surface of the workpiece, shear strain is generated within the near-surface region of the workpiece as a result of the frictional contact. High degree of heat is also generated during the shear deformation [18]. With high level of shear strain, in combination with the elevated temperature, continuous dynamic recrystallization is facilitated [13], resulting in grain refinement within the near-surface region of the workpiece as both the shear stress and the temperature gradients decrease gradually from the machining surface to the bulk region. The fine precipitates are largely dissolved within the near-surface deformed layers during the machining process. Elevated temperature facilitates the dissolution of the precipitate ($MgZn_2$) into the alloy matrix [21]. As the temperature gradient decreases gradually from the machining surface to the bulk region [19], dissolution of the precipitates in greater depth is less likely due to the relatively lower temperature. Thus, such fine precipitates are maintained in the relatively deep region of the deformed layer and the bulk alloy region of the workpiece.

4.2 The impact of machining parameters

It is revealed that the thickness of the near-surface deformed layer increases with increased cutting thickness. This is associated with the force acting on the workpiece by the cutting tool. As illustrated in Fig. 9(a) [22], the resultant force (**R**) acting on the workpiece by the cutting tool can be expressed as: $\mathbf{R}=\mathbf{N}/\cos\beta$, where **N** refers to the normal force exerted on the chip by the tool, and β refers to the friction angle which is related to the coefficient of friction μ ($\mu=\tan\beta$). Once other machining parameters are selected, with higher value of cutting thickness, the thickness of the chip increases and, consequently, normal force (**N**) of higher value is required [18, 23]. The resultant force (**R**) increases as well. With higher value of the resultant force, the friction between the tool and the workpiece beneath the tool also increases. The variation of the resultant force with the increase of cutting thickness is illustrated in Fig. 9(b) and Fig. 9(c), where the cutting thicknesses are indicated by double headed arrows. The friction force ($\mathbf{F_c}$) acting on the machined surface increases along with the resultant force with increased cutting thickness. As the shear stress within the near-surface region is

introduced by the friction force on the surface beneath the tool, higher level of shear deformation occurs within the near-surface region in the workpiece when friction force is larger. According to previous work [24] on stress distribution in orthogonal cutting, shear stress decreases from the surface subjected to the friction force to the bulk region away from the surface, with the maximum shear stress observed on the surface. Relatively high level of shear stress is introduced into deeper region with the increased cutting thickness. Since the grain refinement is closely dependent on the shear stress intensity [7, 13], grain refinement occurs in increased depth when the cutting thickness is increased. In other words, the deformed layer extends to a greater thickness when the workpiece is subjected to orthogonal machining with higher cutting thickness.

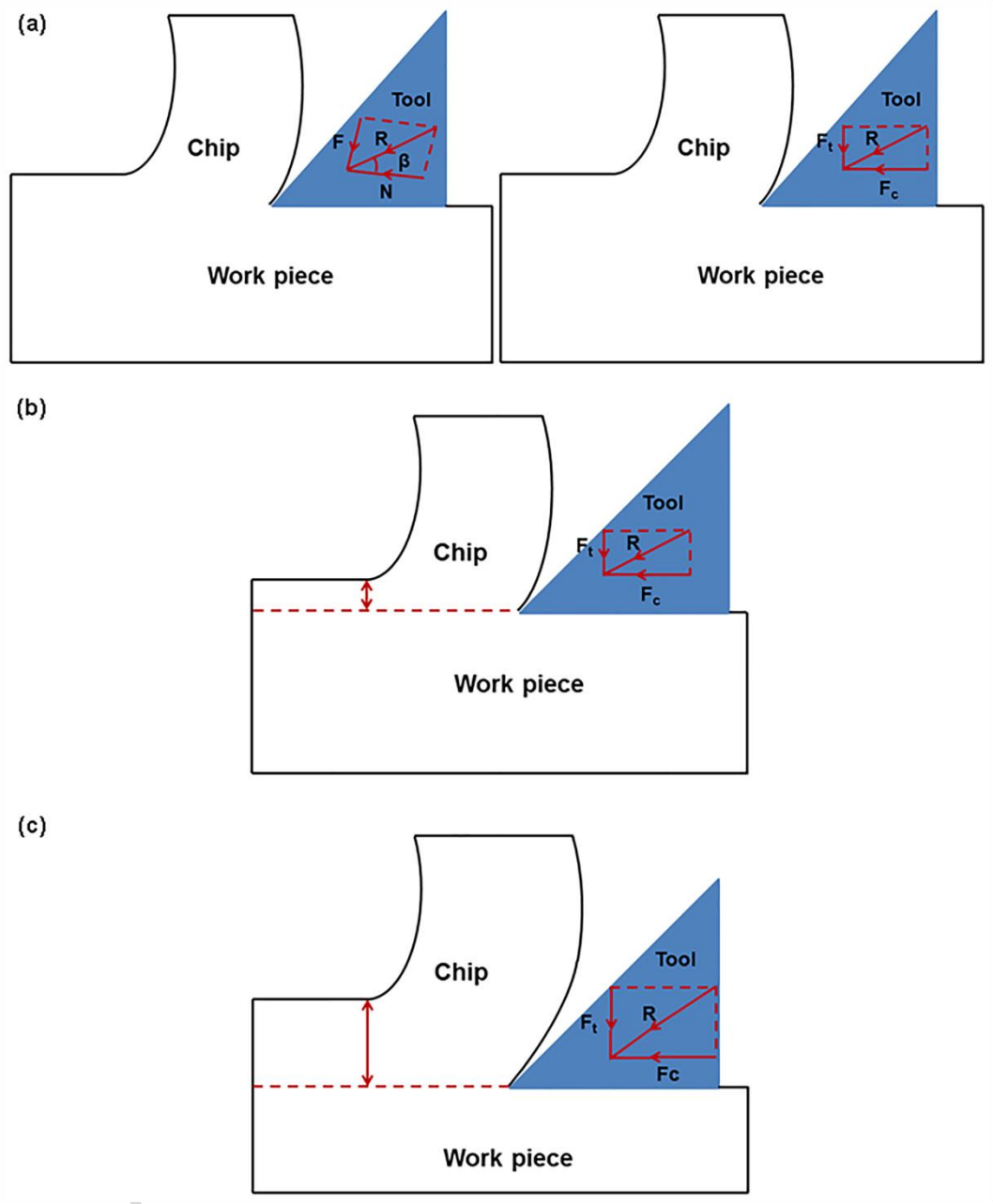

Fig. 9 Schematic diagrams showing: (a) the forces in orthogonal machining [22]; (b) the resultant force with relatively thin cutting thickness; and (c) the resultant force with relatively thick cutting thickness. **R** refers to the resultant force; **N** and **F** represent the normal force and the friction force acting on the chip by the cutting tool; $\mathbf{F_t}$ and $\mathbf{F_c}$ refer to the normal force and the friction force acting on the surface of the workpiece by the cutting tool; and β represents the friction angle.

As revealed in Fig. 4, higher cutting speed results in thicker near-surface deformed layer on the workpiece. This is because higher energy input is involved in the cutting process when a higher cutting speed is employed. When other parameters are selected, the friction force increases with increased resultant force caused by increased cutting speed. Therefore, when a higher cutting speed is employed, higher level of energy is transferred to the workpiece, resulting in higher level of shear deformation and higher temperature in the workpiece. This facilitates the dynamic recrystallization in greater depth and results in a thicker deformed layer [13].

Orthogonal machining with clearance angle of 0 degree results in a near-surface deformed layer with greater thickness compared with 45 degrees clearance angle, as shown in Fig. 5. With 0 degree clearance angle, the contact area between the tool and the workpiece is larger compared with that when the clearance angle is 45 degrees, as illustrated in Fig. 10. Due to the friction between the tool and the workpiece, relatively high shear stress is introduced to the workpiece when the clearance angle is 0 degree [23, 25]. Therefore, the dynamic recrystallization occurs in deeper region, resulting in relatively thick near-surface deformed layer when the clearance angle is 0 degree compared with that when the clearance angle is 45 degrees.

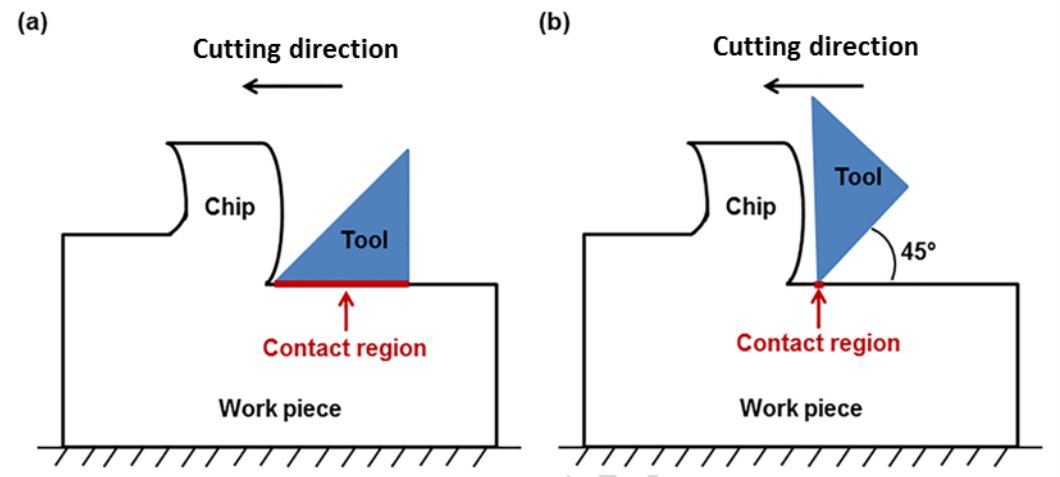

Fig. 10 Schematic diagrams showing the cutting processes with different clearance angles: (a) 0 degree; and (b) 45 degrees.

5. Conclusions

1. Orthogonal machining has been successfully simulated by ultramicrotomy which reproduces the interaction between the tool and the material beneath the tool during the industrial machining process and the associated deformation introduced to the workpiece.
2. Near-surface deformed layers, characterized by ultrafine grains with diameters less than 100 nm, are formed on the AA7150-T651 aluminium alloy subjected to the orthogonal machining.
3. The typical strengthening precipitates $MgZn_2$ in the alloy in the T651 temper are dissolved within the outer region of the deformed layer during the machining process.
4. The thickness of the deformed layer varies from approximately 200 nm to 400 nm, depending on the machining operation parameters. The thickness of the deformed layer increases with increased cutting thickness or higher cutting speed when other machining parameters are fixed. Thicker deformed layer is formed on the workpiece subjected to machining with the clearance angle of 0 degree compared with that with 45 degrees clearance angle.

Acknowledgements

The authors acknowledge the UK Engineering and Physical Sciences Research Council (EPSRC) for supporting LATEST2 Programme Grant and the financial support of the China Scholarship Council.

References

[1] Y. Liu, T. Hashimoto, X. Zhou, G.E. Thompson, G.M. Scamans, W.M. Rainforth, J.A. Hunter, Influence of near-surface deformed layers on filiform corrosion of AA3104 aluminium alloy, Surf. Interface Anal. 45 (2013) 1553-1557.

[2] M.F. Frolish, J.C. Walker, C. Jiao, W.M. Rainforth, J.H. Beynon, Formation and structure of a subsurface layer in hot rolled aluminum alloy AA3104 transfer bar, Tribol. Int. 38 (2005) 1050-1058.

[3] I. Nikitin, I. Altenberger, H.J. Maier, B. Scholtes, Mechanical and thermal stability of mechanically induced near-surface nanostructures, Mater. Sci. Eng. A 403 (2005) 318-327.

[4] J. Wang, X. Zhou, G.E. Thompson, J.A. Hunter, Y. Yuan, Delamination of near-surface layer on cold rolled AlFeSi alloy during sheet forming, Mater. Charact. 99 (2015) 109-117.

[5] Y. Liu, M.F. Frolish, W.M. Rainforth, X. Zhou, G.E. Thompson, G.M. Scamans, J.A. Hunter, Evolution of near-surface deformed layers during hot rolling of AA3104 aluminium alloy, Surf. Interface Anal. 42 (2010) 180-184.

[6] A. Kazemi Talachi, M. Eizadjou, H. Danesh Manesh, K. Janghorban, Wear characteristics of severely deformed aluminum sheets by accumulative roll bonding (ARB) process, Mater. Charact. 62 (2011) 12-21.

[7] X. Zhou, Y. Liu, G.E. Thompson, G.M. Scamans, P. Skeldon, J.A. Hunter, Near-surface deformed layers on rolled aluminium alloys, Metall. Mater. Trans. A 42A (2011) 1373-1385.

[8] M. Fishkis, J.C. Lin, Formation and evolution of a subsurface layer in a metalworking process, Wear 206 (1997) 156-170.

[9] B. Liu, X. Zhou, The impact of machining on the corrosion behaviour of AA7150-T651 aluminium alloy, Mater. Sci. Forum 794 (2014) 217-222.

[10] K. Li, X. Zhou, G.E. Thompson, J. Hunter, Y.D. Yuan, Evolution of near-surface deformed layers on AA3104 aluminium alloy, Mater. Sci. Forum 765 (2013) 358-362.

[11] X. Zhou, G.E. Thompson, G.M. Scamans, The influence of surface treatment on filiform corrosion resistance of painted aluminium alloy sheet, Corros. Sci. 45 (2003) 1767-1777.

[12] Y. Liu, X. Zhou, G.E. Thompson, T. Hashimoto, G.M. Scamans, A. Afseth, Precipitation in an AA6111 aluminium alloy and cosmetic corrosion, Acta Mater. 55 (2007) 353-360.

[13] F.J. Humphreys, M. Hatherly, Recrystallization and related annealing phenomena, Elsevier, Oxford, 2004.

[14] J. Hua, D. Umbrello, R. Shivpuri, Investigation of cutting conditions and cutting edge preparations for enhanced compressive subsurface residual stress in the hard turning of bearing steel, J. Mater. Process Technol. 171 (2006) 180-187.

[15] K. Fuh, C. Wu, A residual-stress model for the milling of aluminum alloy (2014-T6), J. Mater. Process Technol. 51 (1995) 87-105.

[16] J.D. Thiele, S.N. Melkote, Effect of tool edge geometry on workpiece subsurface deformation and through-thickness residual stresses for hard turning of AISI 52100 steel, J. Manuf. Process 2 (2000) 270-276.

[17] J. Limido, C. Espinosa, M. Salaun, J.L. Lacome, A new approach of high speed cutting modelling: SPH method, J. Phys. IV 134 (2006) 1195-1200.

[18] W. Grzesik, Advanced machining processes of metallic materials: theory, modelling and applications, Elsevier, Amsterdam; Boston, 2008.

[19] P. Majumdar, R. Jayaramachandran, S. Ganesan, Finite element analysis of temperature rise in metal cutting processes, Appl. Therm. Eng. 25 (2005) 2152-2168.

[20] J.T. Black, R.A. Kohser, Materials and processes in manufacturing, John Wiley & Sons, Inc., New York, 2008.

[21] Y. Liu, A. Laurino, T. Hashimoto, X. Zhou, P. Skeldon, G.E. Thompson, G.M. Scamans, C. Blanc, W.M. Rainforth, M.F. Frolish, Corrosion behaviour of mechanically polished AA7075-T6 aluminium alloy, Surf. Interface Anal. 42 (2010) 185-188.

[22] J. Beddoes, M.J. Bibby, Principles of metal manufacturing processes, Arnold, London, 1999.

[23] T. Childs, K. Maekawa, T. Obikawa, Y. Yamane, Metal machining: theory and applications, Arnold, London, 2000.

[24] B. McClain, S.A. Batzer, G.I. Maldonado, A numeric investigation of the rake face stress distribution in orthogonal machining, J. Mater. Process Technol. 123 (2002) 114-119.

[25] G. Boothroyd, W.A. Knight, Fundamentals of machining and machine tools, Marcel Dekker, Inc., New York, Basel, 1989.